Interfacing Microwells with Nanoliter Compartments: A Sampler Generating High-Resolution Concentration Gradients for Quantitative Biochemical Analyses in Droplets

ARTICLE *in* ANALYTICAL CHEMISTRY · DECEMBER 2014

Impact Factor: 5.64 · DOI: 10.1021/ac503336g · Source: PubMed

7 AUTHORS, INCLUDING:

Maren Butz
AstraZeneca
5 PUBLICATIONS **54** CITATIONS
SEE PROFILE

Jiří Damborský
Masaryk University
193 PUBLICATIONS **4,000** CITATIONS
SEE PROFILE

Zbynek Prokop
Masaryk University
68 PUBLICATIONS **1,041** CITATIONS
SEE PROFILE

Florian Hollfelder
University of Cambridge
107 PUBLICATIONS **3,594** CITATIONS
SEE PROFILE

analytical chemistry

Article

pubs.acs.org/ac

Interfacing Microwells with Nanoliter Compartments: A Sampler Generating High-Resolution Concentration Gradients for Quantitative Biochemical Analyses in Droplets

Fabrice Gielen,[†] Tomas Buryska,[‡,§] Liisa Van Vliet,[†] Maren Butz,[†] Jiri Damborsky,[‡,§] Zbynek Prokop,[‡,§] and Florian Hollfelder*[,†]

[†]Department of Biochemistry, University of Cambridge, 80 Tennis Court Road, Cambridge, CB2 1GA, United Kingdom

[‡]International Centre for Clinical Research, St. Anne's University Hospital, Pekarska 53, 656 91 Brno, Czech Republic

[§]Loschmidt Laboratories, Department of Experimental Biology and Research Centre for Toxic Compounds in the Environment RECETOX, Faculty of Science, Masaryk University, Kamenice 5/A13, 625 00 Brno, Czech Republic

Supporting Information

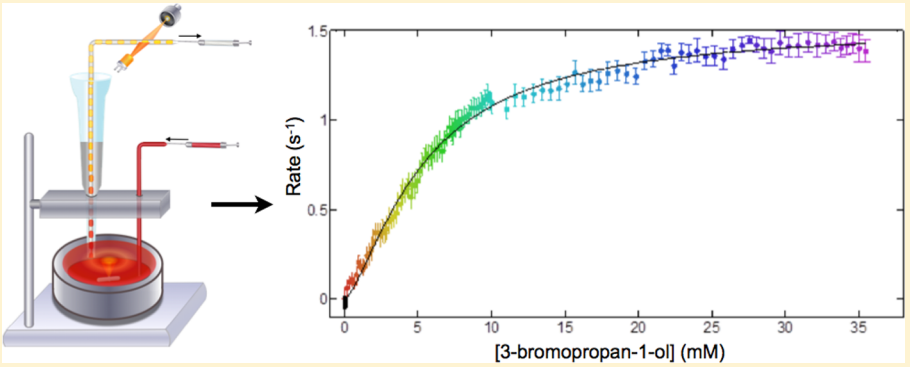

ABSTRACT: Analysis of concentration dependencies is key to the quantitative understanding of biological and chemical systems. In experimental tests involving concentration gradients such as inhibitor library screening, the number of data points and the ratio between the stock volume and the volume required in each test determine the quality and efficiency of the information gained. Titerplate assays are currently the most widely used format, even though they require microlitre volumes. Compartmentalization of reactions in pico- to nanoliter water-in-oil droplets in microfluidic devices provides a solution for massive volume reduction. This work addresses the challenge of producing microfluidic-based concentration gradients in a way that every droplet represents one unique reagent combination. We present a simple microcapillary technique able to generate such series of monodisperse water-in-oil droplets (with a frequency of up to 10 Hz) from a sample presented in an open well (e.g., a titerplate). Time-dependent variation of the well content results in microdroplets that represent time capsules of the composition of the source well. By preserving the spatial encoding of the droplets in tubing, each reactor is assigned an accurate concentration value. We used this approach to record kinetic time courses of the haloalkane dehalogenase DbjA and analyzed 150 combinations of enzyme/substrate/inhibitor in less than 5 min, resulting in conclusive Michaelis–Menten and inhibition curves. Avoiding chips and merely requiring two pumps, a magnetic plate with a stirrer, tubing, and a pipet tip, this easy-to-use device rivals the output of much more expensive liquid handling systems using a fraction (~100-fold less) of the reagents consumed in microwell format.

Extracting quantitative information from chemical and biological experiments is fundamental for structure–activity relationships relevant to fundamental research, as well as for diverse applications in drug discovery, diagnostics, and personalized medicine. High-throughput screening campaigns are limited by the scarcity of test compound material and therefore typically only testing the activity of interest at one (or a few) concentrations of a given compound, leaving more meaningful detailed characterization to low-throughput formats. Currently, the most commonly used screening format relies on 96- or 384-well titerplates (typically using 200 or 40 μL assay volumes, respectively). Most robotic liquid handling systems are specifically interfacing to these plate formats for dispensing and performing serial dilutions. Although new dispensing methods already operate in the pL range (e.g., acoustic dispensing), the final assay volume is still in the microliter range.[1,2] However, the large capital expenditure for robotic sample handlers and analytics make comprehensive data

Received: September 4, 2014
Accepted: November 13, 2014

   dx.doi.org/10.1021/ac503336g | *Anal. Chem.* XXXX, XXX, XXX–XXX

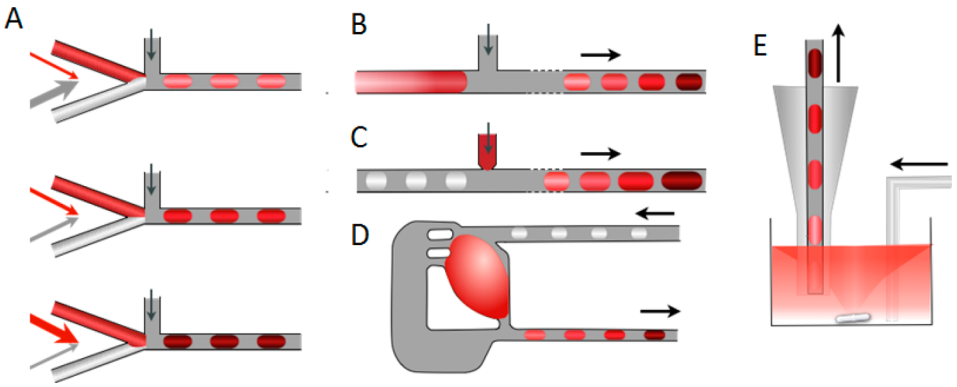

Figure 1. Schematic representation of formats for the generation of series of microdroplets with varying concentrations. Red and light gray coloring represents the sample and diluent that are mixed in varying proportions to bring about a concentration gradient. Dark gray shading represents the oil phase. The arrows indicate the respective flow directions. (A) *Method A*: Adjustment of flow rates of sample and diluent generates droplets with concentrations corresponding to the ratio of the flow rates. The width of the red or light gray arrows represents the magnitude of the flow rates. (B) *Method B:* A continuous-flow concentration gradient is generated in a channel and followed by encapsulation. (C) *Method C*: Injection of a sample into preformed droplets. Droplets can be formed with method A, B, and C at high-throughput (>1 kHz) and with pL volumes. (D) *Method D:* Creation of a series of droplets with changing concentration using a dilution device. (E) *Method E:* Encapsulation of the content of a well whose composition is continuously altered due to injection of sample. Rapid mixing is achieved using a magnetic stir bar. Droplets formed by method D and E are generated at a frequency <10 Hz and have nanoliter volumes.

mining expensive. Technologies that enable the testing of an extended dilution range and can be used "at home" (i.e., implemented straightforwardly and without prohibitively large costs) will shorten the screening pipeline[3] and will be crucial to making high-throughput screening more accessible to a wider circle of scientists.[4]

An effective approach to miniaturization of biological, medical, and chemical assays has been the compartmentalization of individual reactions in micrometer-sized droplets or plugs that offer the possibility to reduce the assay volume to nano- or femtoliters. Water-in-oil microdroplets can be produced at kHz to MHz rates in microfabricated fluidic devices with T-shaped junctions (or similar geometries), with excellent monodispersity.[5−11] When setting up concentration gradients as the basis for dose response analyses, several strategies have been explored.[12,13] These technical solutions differ crucially in (i) the throughput that can be achieved (determining the size of a library of compounds that can be realistically screened), (ii) the precision of and control over the concentration gradients (determining how well concentration-dependent functional data can be measured), (iii) the time taken per experiment, and (iv) the volume consumed per reagent combination (determining the cost of the experiment).

Screening in standard microfluidic chips is slowed down by the time-consuming reloading of microfluidic channels, and alternatives to chip-based encapsulation have emerged. Specifically, the precise definition of the droplet content is possible within droplet-on-demand platforms, whereby pre-programmed sequences of droplets are generated via droplet making robotic heads.[14−19] So far, these platforms have been shown to be highly successful at generating a relatively high number of unique reagent combinations (~100) with the ability to supply *multiple* reagents in succession, albeit only with moderate throughput (typically less than 10 Hz).[20,21] Among these droplet-on-demand platforms, several approaches provide an interface between droplet creation and wells, titerplates, or equivalent sample reservoirs,[14,19,22−24] which enables screening of a large number of experimental conditions as well as straightforward spatial encoding of the droplet content.

Methods for Producing Droplets with Defined Concentrations. The formation of concentration gradients in series of droplets has so far been dominated by four methods: (A) based on multiple injector pumps whose flow rates determine concentrations in droplets (Figure 1A), (B) by converting a concentration gradient resulting from a dispersion profile into droplets (Figure 1B), (C) by injection of reagents into preformed droplets (Figure 1C), or (D) by serial dilution of a droplet leading to stepwise changes in output droplet concentration (Figure 1D).

In the most widely used method A (Figure 1A), the flow rates that deliver a number of reagents determine the concentration gradient based on pump flow. After mixing, the resulting stream is nipped off continuously at the droplet formation point (see black arrows in Figure 1A) to encapsulate its content in droplets, reflecting the concentration gradient set by the pump flow.[16,25] The concentration of reagents in the downstream channel can be programmed through variation of the flow rates of the injection streams that carry each sample. This approach is limited by the accuracy of pumps that control the fluid delivery. The stability of the flows can be difficult to maintain, being usually limited by pulsing of the fluids, which is exacerbated at very low flow rates. Using this method, every step in concentration is accessed serially (requiring pressure adjustment and equilibration), which makes the overall screening rather tedious. Furthermore, the dilution range when operating within a microfluidic chip is typically limited to 2 orders of magnitude.[26]

In Method B, the concentration gradient arises from a dispersion zone (e.g., a Taylor−Aris dispersion pattern). The spatial distribution of solute is strongly dependent on its intrinsic diffusion coefficient. To account for such patterns, the requirement for robust calibration for the concentration profile arises. Concentration encoders have to be carefully chosen in order to match diffusion patterns of the solute of interest. Furthermore, measurements are highly prone to variations due to pressure stability or surface interactions.[13,27] Method C relies on adding discrete volume increments of sample into previously formed droplets. Control over the injected volume via pressure enables the stepwise change in sample concentration in the

dx.doi.org/10.1021/ac503336g | *Anal. Chem.* XXXX, XXX, XXX−XXX

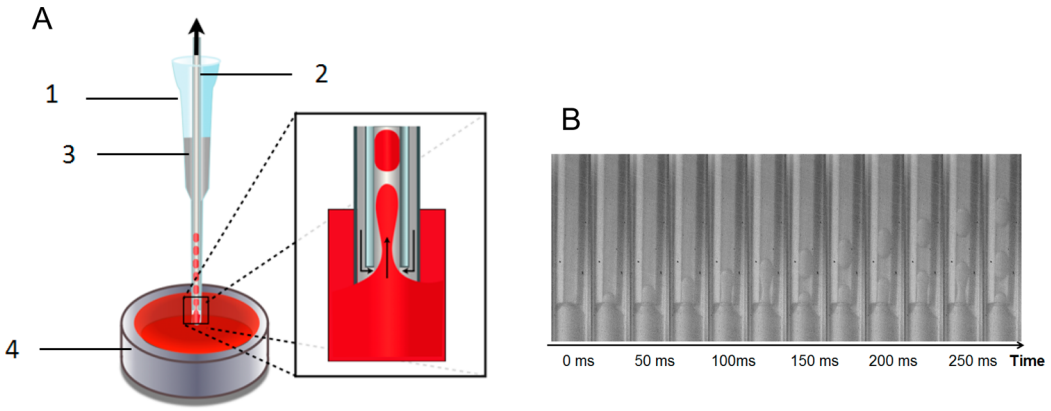

Figure 2. Design of an interface between open microwell and a vertical droplet generator. (A) *Schematic of the droplet generation system.* It includes a pipet tip (1) with a final diameter lower than the tubing o.d., typically a 200 μm i.d., 400 μm o.d. PTFE tubing (2). The tip is filled with 20 μL of fluorous oil HFE-7500 (3) and the well of a titer plate with 40 μL of sample in a 384 well plate (4). When applying a negative pressure to the tubing, the pressure field is applied to both carrier phase and aqueous. The oil/aqueous interface is deformed in squeezing regime and subsequent breakage of the interface ensues to form droplets that protrude into the tubing. (B) *Snapshots of droplet generation* at a withdrawal flow rate of 9 μL/min, taken at intervals of 25 ms. The resulting droplets are monodisperse when a constant flow rate is applied.

droplet that has been injected. The limitations of this approach include contamination of the injection channel with the contents of the droplets and the volume fraction that can be added typically covers less than 2 orders of magnitude.[28,29]

Method D is using a large droplet ("mother" droplet) that gets progressively diluted by merging input droplets containing diluent and budding off "daughter" droplets creating a dilution series.[14,15,26] The concentration range is limited by the volume and respective concentrations of the "mother droplet" and the "diluent" droplets.[26,30]

These four methods have a considerable degree of engineering complexity,[18,31] which has thus far prevented their widespread use. Other, simpler methods to alter droplet-by-droplet composition (for instance, using tubing with cut trenches) have been developed,[32] but—thus far—can alter droplet composition only with limited reproducibility. We now add a novel method (E), implement it using a device manually assembled from inexpensive components, and generate label-free concentration gradients from a source well in which the content is varied by dilution over time. Using such devices, each droplet in a sequence can be assigned an accurate concentration value based solely on its time tag (i.e., the time at which the droplet has been withdrawn from a sample reservoir with controlled contents), making the use of encoders superfluous. This device can be readily interfaced with titerplates, as well as with microfluidic chip technology. Quantitative measurements in monodisperse nanolitre reactors that give rise to structure–activity relationship for small molecules, enzymes, or single cells thus become economical and straightforward.

RESULTS AND DISCUSSION

Design of a Microplate/Microdroplet Interface. Our droplet generation design relies on withdrawal of liquid into a capillary to achieve flow segmentation at the same time as withdrawing sample. The segmentation is based on aligned microcapillaries but uses a negative pressure source instead of multiple positive pressure inputs.[7] This feature of a double lumen configuration is similar to a previously reported device[33] but makes use of a single negative pressure source to withdraw sample and carrier fluid simultaneously. The droplet-making unit can be held vertically and is immersed in an open well filled with an aqueous solution, enabling direct interfacing with the widely used titer plate storage and screening format (Figure 1E).

A pipet tip serves as a circular microchannel of gradually decreasing inner diameter (i.d.)—the initial at its top i.d. is 5 mm, while the final i.d. at its bottom is 360 μm. A polytetrafluoroethylene (PTFE) tubing of matching dimensions (typically i.d. of 200 μm, outer diameter (o.d.) 400 μm) is manually inserted into the pipet tip (Figure 2A). Once the tubing is fully inserted, it is held in place by friction forces with the walls of the tip, and the carrier oil phase can be dispensed inside the tip. After applying negative pressure to the tubing, the fluid placed at the narrow end of the tip is sucked up and will be passively split into microsegments. Plugs will be formed when the annular gap between tip and tubing provides sufficient surface area for the oil phase to enter the tubing. This arrangement may require small adjustments of the height of the inner tubing (Figure S2). The assembly of such samplers is typically complete in a few minutes and was performed for each experiment. Reproducibility in generating droplets was found to be excellent. However, a precise droplet volume cannot be set *a priori*: the lack of accurate positioning inside the tapered tip means that the envisaged droplet volume can only be approximated, although near-monodisperse series of droplets are generated.

The overall configuration resembles a coflow geometry,[7,34] but the droplet formation mechanism involves an elongational squeezing phase.[35] This phase is apparent in the snapshots shown in Figure 2B, implying that the oil in effect provides a perpendicular viscous shear force during its 180° turn, pinching the aqueous interface, while a droplet is advancing inside the tubing until pinch-off. As such, the operation is similar to a flow-focusing geometry.[36,37]

Here the negative pressure withdraws both aqueous and oil phase. The relative resistance of the paths are dictated by the surface areas available to both.[38] This vertical droplet generation unit requires only a pipet tip, PTFE tubing and a syringe pump operating in withdrawal mode, making it much easier to construct than classical microfluidic chips (see Figure S1).

Fluidic Calibration To Govern Droplet Size and Production Rate. Droplet monodispersity was maintained using a 40 cm-long tubing line (accommodating ~400

dx.doi.org/10.1021/ac503336g | *Anal. Chem.* XXXX, XXX, XXX–XXX

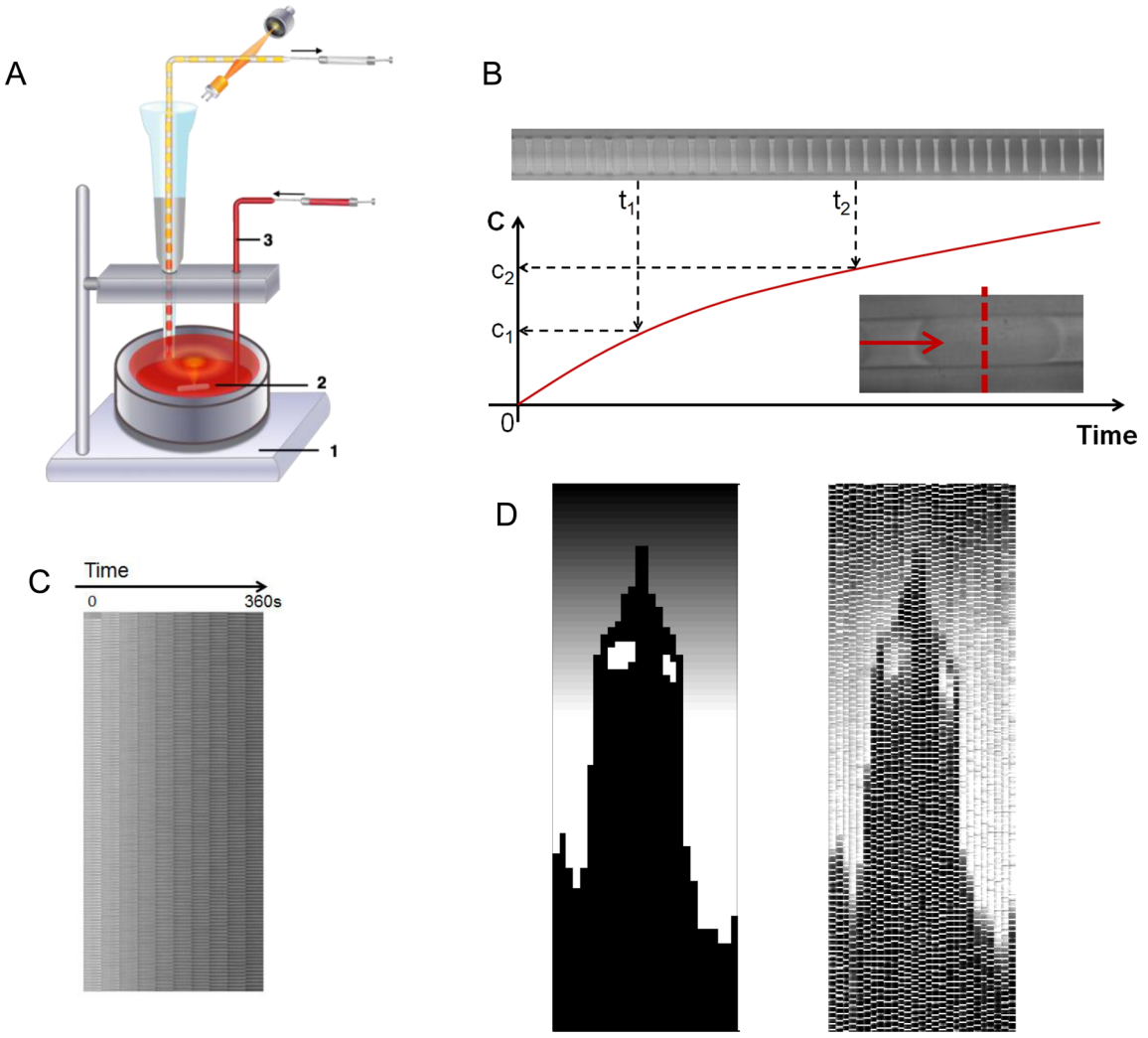

Figure 3. Programming of precisely controlled concentration gradients. (A) Schematic of the configuration for the precise conversion of the stock concentration in the well into a desired concentration in a droplet. The open well sits on top of a magnetic stirrer (1). The solute concentration is continuously added using a tubing (3) connected to a syringe pump and the well content stirred via a magnetic stir bar (2). The pipet tip is cut right at the narrow end of the tubing to minimize dispersion. In this way, the sample present in the well at a given time will be typically encapsulated within one second. (B) Assembled cross sections of the tubing over time showing the contents of droplets as they change. The cross-section and direction of flow is shown in the snapshot as a red dotted line and a red arrow. The concentration of each droplet can be calculated based on the flow rates for withdrawal, injection, initial volume and concentration of the sample (following eq 1). (C) Example of a concentration gradient with increasing phenol red concentration (ranging between 0 and 230 μM) across a total of approximately 1100 droplets. A fixed cross-section of each video frame was taken and assembled to produce separate bands which represent individual droplets that appear compressed. Each column was set to contain 36 s of video, corresponding to approximately 110 droplets. Phenol red solution (1 mM in 50 mM Tris/HCl buffer, pH 7.5) was injected at a flow rate of 10 μL/min for 6 min into a 96-well plate that was filled initially with 200 μL buffer (50 mM Tris/HCl buffer, pH 7.5). Droplets were generated at a rate of around 3 Hz. (D) A programmed sequence of droplets demonstrates precise time control over droplet content. The graphical pattern of the image on the left (showing the London landmark Big Ben) was replicated as a collection of droplets with a concentration-controlled dye pattern (shown on the right). An extra pump was used to inject buffer to the well enabling dilutions. The overall setup is shown in Figure S6. The image was resolved as a sequence of serial dilutions to form the input into a single Labview program controlling the pumps and their timing. The resulting movie file has been resliced and columns assembled to reconstruct the final picture. The recording time for the movie was around 40 min. The movie at 200× speed and synchronized reconstruction of the image can be found in the SI (Video 4a and Video 4b).

droplets) for more than 30 min at production rate of 2 Hz with a typical polydispersity for the effective droplet radius of 6% (Figure S5), corresponding to ∼18% volume difference. This is higher than for classical positive pressure flow focusing device (less than 3%) because of the pressure fluctuations due to the presence of an increasingly long droplet sequence in a tubing and fluid compressibility (often leading to the appearance of air bubbles).[7,39] This method is able to generate droplets ranging from 200 pL (with a 50 μm i.d. tubing) to 50 nL (with a 200 μm i.d. tubing) at rates between 0.1 and 12 Hz. At fixed tubing location, the plug length increased with increasing flow rates until only water was withdrawn (Figure S2 and SI, Video 1). When the tubing was held in a higher position, more surface area was available to the oil phase, and therefore, higher flow rates were necessary to generate water droplets. Frequencies of up to 12 Hz (flow rate of 20 μL/min) were reached with a 200 μm i.d. tubing, HFE-7500 oil and water. The droplet generation shows only a weak dependency on the volume of oil in the tip above 2.5 μL (Figure S3). Other carrier phases able to wet the tip and tubing can be used without affecting the ability to

dx.doi.org/10.1021/ac503336g | *Anal. Chem.* XXXX, XXX, XXX−XXX

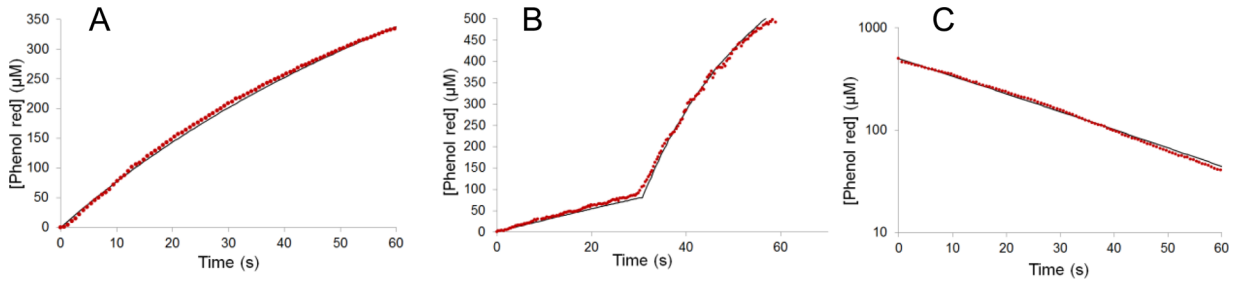

Figure 4. Superposition of the analytical concentration profile (black) and the measured concentrations (red). For all curves, the diluent was PBS buffer (pH 7.4), and the solute was phenol red. Absorbance detection was performed at 590 nm using fiber optics aligned with the tubing as previously described.[14] (A) One-step infusion: droplets were generated over 60 s. Flow rates for withdrawal and infusion were 3 and 25 μL/min, respectively. Start volume was 150 μL. (B) Two-step infusion: droplets were generated for 30 s at 25 μL/min followed by 30 s at 250 μL/min into an initial volume of 150 μL. (C) Reverse dilution using a third syringe pump withdrawing fluid at the same time as buffer was being injected. The initial phenol red concentration was 500 μM with well volume of 40 μL. Flow rates were 100 μL/min for the infusion and withdrawal and 3 μL/min for droplet generation.

generate droplets. For instance, mineral oil can be used in replacement of fluorous oil (see SI, section S1.4). A drop of low microliter volume (here 2 μL) can also be fully sampled into nanoliter segments (SI, Video 2).

Creation of Label-Free Concentration Gradients in a Series of Droplets. Dilution series with freely adjustable, distinct concentrations in individual droplets can be set up by placing the first component in the well (e.g., a solvent) and infusing the second component (e.g., a solute) to the same well. Instant mixing of the two components is ensured by placing the outlet of the infusion tubing close to a magnetic stirrer, while droplets are formed by sample withdrawal at the same time (Figure 3A). Consequently, the droplet contents represent a time capsule corresponding to the composition of the well. The final concentration is freely adjustable and solely controlled by the fluidic parameters (volumes, flow rates) provided it does not surpass solubility limit. The number of droplets and their content, generated before reaching the target concentration (the "gradient" droplets) also rely solely on these fluidic parameters. Thus, the concentration of the components in each of a droplet series is preplanned and droplets are "encoded" by their order, making labels superfluous.

The replacement of labels by "time encoding" contrasts this method to other techniques for creating gradients, especially those relying on the formation of dispersion zones before encapsulation.[13,27] Here, we minimize continuous flow dispersion effects by transforming an aqueous sample into a droplet via a small dispersion volume (<100 nL), which the sample typically passed for less than 1 s (at 3 μL/min). We achieved this low dispersion volume by cutting the tip as close as possible to the fully inserted tubing (typically less than 1 mm apart). The cutting can be fine-tuned by producing air plugs in oil to precalibrate the formation of aqueous plugs (SI, Video 3).

Two design features—fast homogenization of the well and droplet formation very close to the bulk of the well—thus enable the formation of concentration gradients with excellent control over the contents of individual compartments.

Formal Expression for Calculation of the Droplet Concentration. The concentration of the ingredients within each compartment can be assigned analytically, on the basis of the known sample condition in the well. Assuming ideal mixing, ideal pump responses and instantaneous transfer of matter from well to droplet, concentrations can be calculated as a function of time t from the start of the injection process, the withdrawal flow rate (q_{out}) of the aqueous phase and the infusion flow rate (q_{in}), and the initial volume present in the well (V_i). The rate of change in the quantity of the injected solute n_2 (in moles) is equal to the difference between the quantity withdrawn and the quantity added giving the following relationship that describes the concentration in the droplet at each time point (c_2) as a function of the injected concentration ($c_{2,i}$) (see SI, S2.1):

$$c_2(t) = \frac{n_2(t)}{v(t)} = c_{2,i}\left[1 - \left(\frac{V_i}{(V_i + (q_{in} - q_{out})t)}\right)^{(q_{in}/q_{in}-q_{out})}\right] \quad \text{(eq 1)}$$

Droplet contents can be modified by altering the concentration of the sample in the well from which they are made and subsequently analyzed on the basis of their order of production (Figure 3B). Concentration gradients with more than 1000 data points can be obtained (Figure 3C) by infusing the second component for longer periods (here 6 min), although storing large numbers of droplets while keeping spatial encoding requires longer tubing lengths (droplet density is typically 1−3 droplets per mm) or a connection to a dedicated microfluidic chip. Additionally, sequential dilutions can be preprogrammed from the same well by injecting either a solute or its buffer. Here we demonstrate the formation of 66 serial concentration gradients, which, when "resliced" into columns, reproduce the pattern of the picture shown in Figure 3D. Visual inspection of the original and the droplet-rendition of the image demonstrate how accurately the dilution system operates.

Accuracy in Assignment of Concentration. In this approach, each droplet reflects the concentration of the solute in the well with a small time shift. The time shift is due to the finite mixing time as well as the presence of a small dispersion zone between the solution of the well and the end of the tubing. To address the quantification of this effect, the response to a step increase in solute concentration has been studied (Figure S7) and shows a response time of less than 1 second to reach 90% of the step increase at a flow rate of 3 μL/min. The sensitivity to misjudging the exact starting point of the concentration gradient shows that after an initial large error, the uncertainty drops exponentially with the progress of the experiment (Figure S8). To circumvent the problem of the precise identification of the start of the dilution, the flow rate of withdrawal was slightly changed (within 20% of the initial flow rate) at the same time as the injection was initiated to produce droplets with a visibly different size. Due to this step change in

dx.doi.org/10.1021/ac503336g | Anal. Chem. XXXX, XXX, XXX−XXX

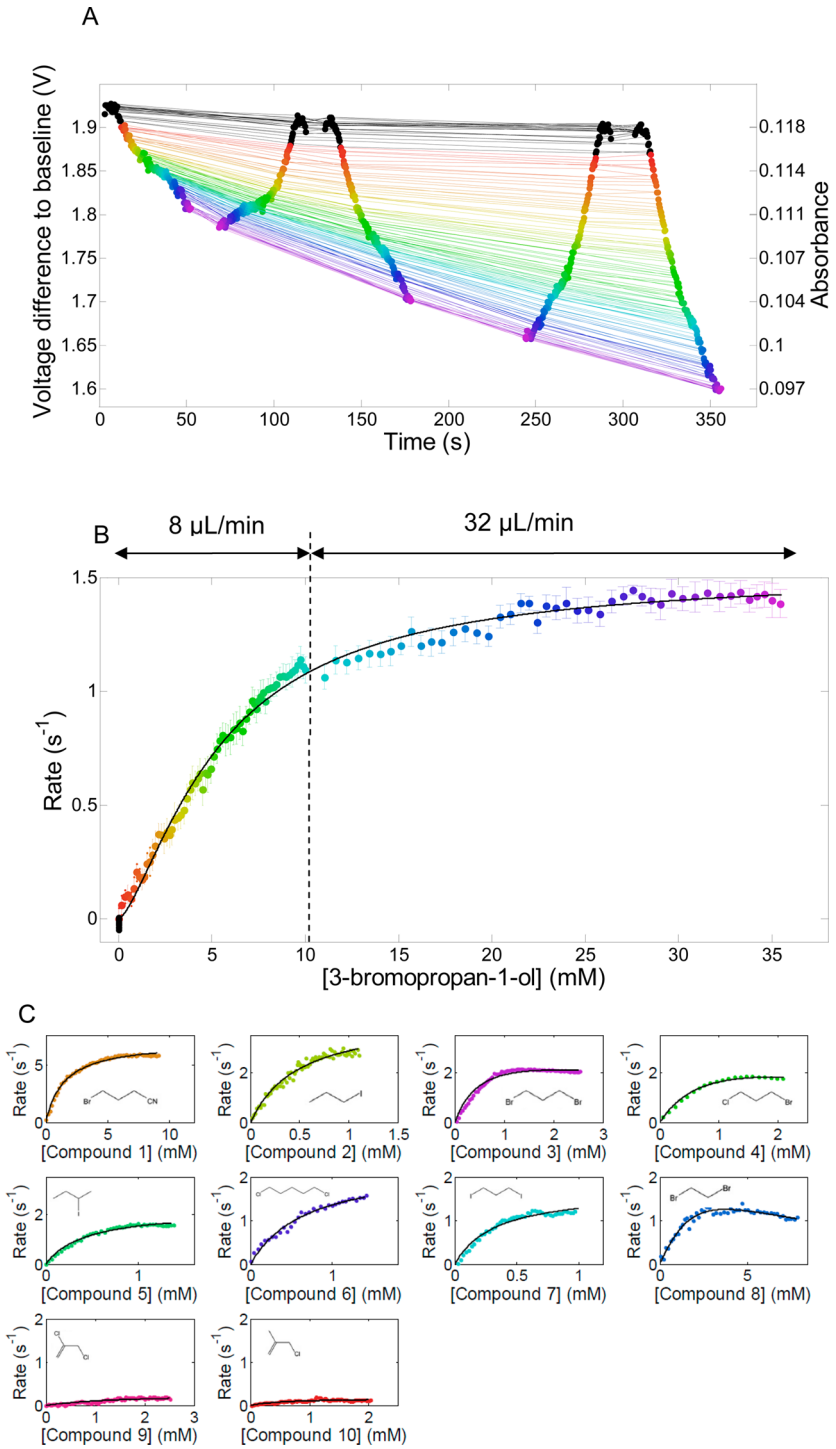

Figure 5. Kinetic data for the reaction enzyme-catalyzed turnover of 3-bromopropan-1-ol (SI, S3) and other promiscuous substrates by the haloalkane dehalogenase DbjA. (A) Time courses monitoring two-step injection kinetics (1st step: 8 μL/min, 2nd step 32 μL/min). Droplet absorbance levels over time for 137 droplets containing increasing concentrations of substrate were read 6-times in 425 s. (B) Initial rates were extracted from slopes in A and plotted against substrate concentration. The switch from slower (8 μL/min) to higher flow rates (32 μL/min) was calculated to be close to 10 mM in substrate concentration. There are 137 points with enzyme and substrate concentrations ranging in the two regimes (800−720 nM and 0 to 36 mM, respectively). The kinetic data were fit to the Michaelis−Menten equation yielding a K_m of 5.4 ± 0.2 mM and k_{cat} of 1.52 ± 0.03 s^{-1} (close to values measured in a titerplate assay (Figure S9).[45] (C) Michaelis−Menten plots for 10 haloalkane substrates tested with DbjA with the fits superimposed. The kinetics parameters can be extracted with high accuracy (SI, Table 1). Compound names are as follows: (1) 4-bromobutyronitrile, (2) 1-iodopropane, (3) 1,3-dibromopropane, (4) 1-bromo-3-chloropropane, (5) 2-iodobutane, (6) 1,5-dichloropentane, (7) 1,3-diiodopropane, (8) 1,2-dibromoethane, (9) 2,3-dichloropropene, (10) 3-chloro-2-methylpropene. The total time taken for generating these 10 plots was 50 min.

droplet length, the start time of the dilution can thus be easily assigned.

A dilution series of the colored dye phenol red (dissolved in PBS, pH 7.4) indicates excellent agreement between exper-

dx.doi.org/10.1021/ac503336g | Anal. Chem. XXXX, XXX, XXX−XXX

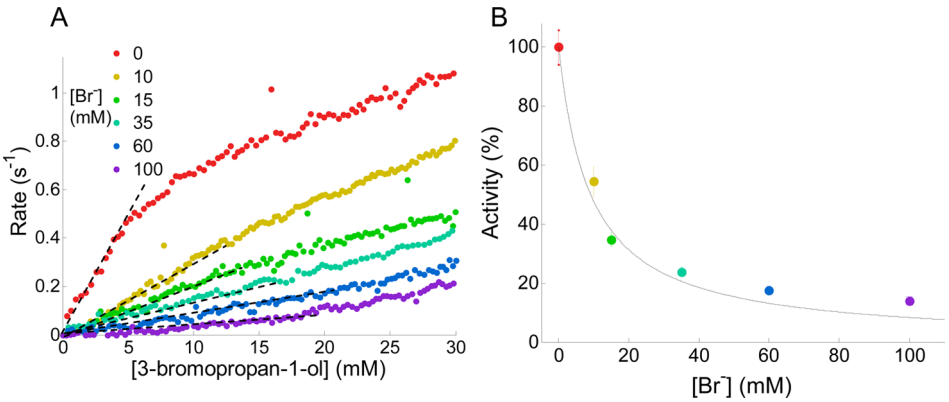

Figure 6. Kinetic analysis of enzyme inhibition. (A) Rates of the reaction of 3-bromopropan-1-ol catalyzed by DbjA in the presence of various concentrations of bromide (acting as an inhibitor). Each data point corresponds to the initial slope of a time course (panel A). (B) Relative k_{cat}/K_m values versus concentration of bromides used as an inhibitor. The black line represents the best fit of kinetic data using eq 2 (see description in SI). Each data point in panel B represents the slope of the linear portion of Michaelis–Menten curves taken from panel A (represented by dashed black lines).

imental and calculated dilution profiles (according to eq 1) with deviations below 10% over the whole concentration range (Figure 4A), except for the five first droplets. If several concentration bands are needed, a multistep infusion can be preprogrammed to cover this wider concentration range (Figure 4B). Even exchanging components (decreasing one while increasing the other) is possible with a reverse dilution. This can be achieved with a well initially filled with a first component that is diluted by a second component. Simultaneous with the injection, the same amount of volume is pumped out of the well using a third syringe pump (Figure 4C) to keep the overall volume constant.

Dynamic Range of the Dilution Operation. The device can be used to either progressively *increase* the concentration of a sample, or *dilute* a sample initially present in the well. For the increase, the smallest achievable concentration increment/step is determined by both the droplet size and the droplet formation frequency. The higher the frequency and the smaller the droplet size, the more individual data points are generated and the larger the concentration range will be. A calculation based on volume ratios illustrates the dynamic range that becomes accessible: if we assume that the injection tubing has an internal diameter of 200 μm, the minimum reliable volume that can be injected is around 10 nL. Using a 384-well plate, 40 μL can be used as starting volume (added to the well already occupied by the stirring bar). This represents a 4000-fold dilution. For a starting volume of 150 μL (i.e., one well of a 96-well plate), the same calculation would give a 1:15 000 dilution. The maximal injectable volume is limited by the overall well size but can reach 300 or 50 μL for 96- and 384-well titerplates, respectively. The concentration range that can be covered extend to more than 3 orders of magnitude (from $2.5\cdot10^{-4}\times$ to 0.5× of the stock concentration). Further expansion of this range can conceivably be achieved by using smaller injection tubing and more accurate pumps to achieve even higher dilution factors (i.e., making 2–3 additional orders of magnitude accessible). The dilution of the sample initially present in the well continues as long as the diluent is replacing the initial sample by typically 1 order of magnitude per minute under the conditions outlined in (Figure 4C). Interestingly, the concentration change of the initial solute can be kept low when the overall volume change is small. The ultimate limitation is therefore the solubility of the compound that is being injected.

Application to Enzyme Kinetics Followed by a Colorimetric pH Indicator Assay. Enzymatic mechanisms are studied by measuring the reaction rate as a function of substrate concentration. Conventional techniques for enzyme kinetic measurements require running separate reactions for each concentration monitored. This strongly limits the number of points included in steady-state kinetic data (while at least some ten points have to be determined for a fit of saturation profiles), or a single activity measurement for each substrate in the case of monitoring a large set of compounds. Encapsulation of the concentration gradient from only one reaction mixture by sampling allows collection of more than 10-fold more kinetic points for one reaction in less than 1 min. The larger number of collected data points leads to determination of the kinetic constants with high precision and potentially covers a wider range, which is advantageous when the precise shape of the nonlinear curve is unknown *a priori*.

We demonstrate how kinetic measurements can be conducted with the haloalkane dehalogenase DbjA from *Bradyrhizobium japonicum* USDA110, an enzyme class with potential applications in biocatalysis, bioremediation, decontamination, biosensing, and molecular imaging.[40−43] One reaction product is $[H^+]$, which can be detected with the help of a pH indicator (such as phenol red, in a modification of Holloway's pH indicator assay[44]). Here, we used a prefilled well with a given amount of enzyme and injected a substrate, so that droplets with quasi-constant enzyme and increasing substrate concentration were produced. The resulting droplet series was stored in tubing and the emergence of product determined by an absorbance detector. The calibration curve for converting absorbance of phenol red into $[H^+]$ was monitored as a change in absorbance at 590 nm. The absorbance profile showed a linear dependency with concentration of added $[H^+]$ in a range from 20 to 625 μM. The minimum detectable concentration was around 10 μM (Figure S10).

Reading of the droplet sequences was accomplished by a previously reported absorbance detection unit that monitors transmittance, consisting of two aligned optical fibers placed directly on the tubing.[14] It is possible to cover the whole substrate range for a full Michaelis–Menten plot (with more data points to describe the curvature at low substrate concentrations and fewer at higher concentrations). This was implemented by programming a two-step substrate injection

dx.doi.org/10.1021/ac503336g | *Anal. Chem.* XXXX, XXX, XXX−XXX

(Figure 5A,B; the raw data for the 137 droplets are shown in Figure S11).

From the Michaelis–Menten plot generated with droplets (Figure 5B), we extracted values for K_m of 5.4 ± 0.2 mM and for k_{cat} of 1.52 ± 0.03 s^{-1}, which approximate results from the same assay run in a titerplate (yielding a K_m of 1.7 ± 0.3 mM and a k_{cat} of 0.5 ± 0.3 s^{-1}; Figure S9). We extended the study to the screening of 10 haloalkane substrates and derived the kinetic parameters (Figure 5C and SI, S6). Comparison of kinetic parameters obtained from gas chromatography measurements indicate good correlation (SI, Table 1), suggesting that the data produced using our microsampling method faithfully reflect kinetics obtained with other techniques. The remaining differences in K_m can be ascribed to possible variation in the evaporation of the volatile substrate in the two procedures.

Such data are suitable as the basis of quantitative structure–activity relationships.[46] The technical facility of obtaining steady-state kinetic profiles in miniaturized experiments allows monitoring of a large range of substrates in full kinetic detail, in this case characterizing a wider range of substrates to profile the broad-specificity of promiscuous enzymes with a full set of steady-state parameters that make systematic evaluation of the recognition characteristics possible and provide a useful starting point for directed evolution.[47−49]

Finally, the characterization of product inhibition by bromide ion (Figure 6) was demonstrated.[50] To this end, the inhibitor was premixed with enzyme, and substrate was injected as described before. These measurements yielded a K_i of 9.1 ± 1.6 mM (using eq 2 in SI, S5), which corresponded well with the K_i of 10.5 ± 6 mM measured in a microtiter plate.

Scope and Limitations of Kinetic Measurements in This Format. The following points summarize the practical conditions when enzyme kinetics measurements in droplets can be accurately obtained.

(i) The time delay between the effective start of the reaction and the formation of the last dilution droplet was typically 30–45 s, implying that some product formation had already taken place. In cases of fast kinetics, this can be accounted for mathematically, by using the integrated form of the rate equations.[51]

(ii) The time interval between consecutive measurements depends on the sequence length and the reading speed. Here 100 droplets were typically read in intervals of 30 s but faster back-and-forth transitions can further reduce this interval. How fast these transitions can occur will ultimately be limited by the time to reach pressure steady-state inside the tubing. Parallel detection schemes or droplet imaging can bypass this limitation.[52,53]

(iii) The absorbance change has to be above the detection limit (of ∼2 × 10^{-4} absorbance units, corresponding to $[H^+]$ = 10 μM). For very active enzymes, the enzyme concentration, where an initial rate can be determined on a time scale of several minutes, has to be experimentally identified. For slow enzymatic reactions, droplets can be stored and read in the tubing for periods up to days without significant evaporation or change in the read order. Thus, there are no limits for slow measurements imposed by the operation of this device.

CONCLUSIONS

The enormous potential of microdroplet technology for high-throughput screening with its self-evident advantages of extremely miniaturized volumes, automation, and the ability to extract information on large collections of samples rapidly has created a powerful new experimental paradigm for high-throughput assays.[6,9,54] However, the technical complexity of the devices and their operation is a significant implementation barrier in laboratories with mainly biological or chemical expertise. For screening in the pharmaceutical industry, the issue of interfacing microfluidic chips with universally adapted multiwell plate formats (such as those typically handled by robotic fluid handling systems) has to be addressed. Our work suggests a way forward to connect these two formats: we demonstrate a straightforward method using standard laboratory equipment that produces useful data to measure enzyme kinetics and determine inhibition constants with a quality that matches data from microwell experiments (despite the 10 000-fold lower volumes). The overall assembly of this device does not require specialized knowledge but relies on standard laboratory parts. An extension of the capabilities of this sampler to automated screening of titerplates is conceivable, for example, by using multirack syringe pumps and parallelized detection schemes.

Data obtained with this device may provide the basis for future screening campaigns to derive not only "hits" from screening of large libraries, but also deliver data that can be the basis of detailed structure–activity relationships. Quantification of the strength of protein–protein interactions and dose–response curves based on single cells or cell populations encapsulated in droplets[55,56] can be imagined. All advantages of the microdroplet format are preserved: the total volume used in each experiment is typically 15 nL per droplet (multiplied with the number of droplets, e.g. resulting in 1.5 μL for 100 data points). The good correlation between theoretical and experimental drop-by-drop concentration gradients ensures high data quality. The "information yield" per total volume is high, because more data points can be sampled in concentration regimes that define a diagnostic curve (i.e., regions of nonlinearity), while fewer can be taken elsewhere (i.e., in linear regions or as saturation is approached in a Michaelis–Menten plot). The ability to generate high-resolution label-free concentration gradients coupled to kinetic measurements sets the scene for automatic high-quality characterization of chemical and biochemical interactions and lowers the barrier to a precise quantitative insight into biomolecular interactions on a scale that is already routine in "omics" and systems biology approaches.

ASSOCIATED CONTENT

Supporting Information

Technical details describing device operation, error analysis, analysis of raw data and comparison of kinetics based on optical detection with product analysis by GC are included. Videos showing the operation of the device and the production of the Big Ben drawing of Figure 3D are also available. This material is available free of charge via the Internet at http://pubs.acs.org.

AUTHOR INFORMATION

Corresponding Author

*E-mail: fh111@cam.ac.uk.

Notes

The authors declare no competing financial interest.

■ ACKNOWLEDGMENTS

This research was funded by the Engineering and Physical Sciences Research Council (EPSRC), the European Research Council (ERC), the European Commission (REGPOT 316345), and the European Regional Development Fund (CZ.1.05/1.1.00/02.0123). F.H. was an ERC Starting Investigator. L.D.V. was supported by a BBSRC Enterprise fellowship and M.B. by a fellowship from the Schweizerischer Nationalfonds. T.B. was supported by FNUSA-ICRC Human Bridge: Incubator of Young Talents III (CZ.1.07/2.3.00/20.0239), the European Social Fund and the State Budget of the Czech Republic (LO1214). The authors thank Charles Baroud and Etienne Fradet for useful discussions.

■ REFERENCES

(1) Haeberle, S.; Zengerle, R. *Lab Chip* **2007**, *7*, 1094.
(2) Marx, V. *Nat. Methods* **2014**, *11*, 33.
(3) Macarron, R.; Banks, M. N.; Bojanic, D.; Burns, D. J.; Cirovic, D. A.; Garyantes, T.; Green, D. V. S.; Hertzberg, R. P.; Janzen, W. P.; Paslay, J. W.; Schopfer, U.; Sittampalam, G. S. *Nat. Rev. Drug Discovery* **2011**, *10*, 188.
(4) Bleicher, K. H.; Bohm, H. J.; Muller, K.; Alanine, A. I. *Nat. Rev. Drug Discovery* **2003**, *2*, 369.
(5) Kintses, B.; van Vliet, L. D.; Devenish, S. R. A.; Hollfelder, F. *Curr. Opin. Chem. Biol.* **2010**, *14*, 548.
(6) Schaerli, Y.; Hollfelder, F. *Mol. Biosyst.* **2009**, *5*, 1392.
(7) Utada, A. S.; Lorenceau, E.; Link, D. R.; Kaplan, P. D.; Stone, H. A.; Weitz, D. A. *Science* **2005**, *308*, 537.
(8) Shim, J. U.; Ranasinghe, R. T.; Smith, C. A.; Ibrahim, S. M.; Hollfelder, F.; Huck, W. T. S.; Klenerman, D.; Abell, C. *ACS Nano* **2013**, *7*, 5955.
(9) Guo, M. T.; Rotem, A.; Heyman, J. A.; Weitz, D. A. *Lab Chip* **2012**, *12*, 2146.
(10) Link, D. R.; Grasland-Mongrain, E.; Duri, A.; Sarrazin, F.; Cheng, Z. D.; Cristobal, G.; Marquez, M.; Weitz, D. A. *Angew. Chem., Int. Ed.* **2006**, *45*, 2556.
(11) Rosenfeld, L.; Lin, T.; Derda, R.; Tang, S. K. Y. *Microfluid Nanofluid* **2014**, *16*, 921.
(12) Dertinger, S. K. W.; Chiu, D. T.; Jeon, N. L.; Whitesides, G. M. *Anal. Chem.* **2001**, *73*, 1240.
(13) Cai, L. F.; Zhu, Y.; Du, G. S.; Fang, Q. *Anal. Chem.* **2012**, *84*, 446.
(14) Gielen, F.; van Vliet, L.; Koprowski, B. T.; Devenish, S. R. A.; Fischlechner, M.; Edel, J. B.; Niu, X. Z.; deMello, A. J.; Hollfelder, F. *Anal. Chem.* **2013**, *85*, 4761.
(15) Churski, K.; Michalski, J.; Garstecki, P. *Lab Chip* **2010**, *10*, 512.
(16) Cao, J. L.; Kursten, D.; Schneider, S.; Knauer, A.; Gunther, P. M.; Kohler, J. M. *Lab Chip* **2012**, *12*, 474.
(17) Du, W. B.; Sun, M.; Gu, S. Q.; Zhu, Y.; Fang, Q. *Anal. Chem.* **2010**, *82*, 9941.
(18) Gu, H.; Murade, C. U.; Duits, M. H. G.; Mugele, F. *Biomicrofluidics* **2011**, 5.
(19) Wu, J. B.; Zhang, M. Y.; Li, X. L.; Wen, W. J. *Anal. Chem.* **2012**, *84*, 9689.
(20) Kintses, B.; Hein, C.; Mohamed, M. F.; Fischlechner, M.; Courtois, F.; Leine, C.; Hollfelder, F. *Chem. Biol.* **2012**, *19*, 1001.
(21) Huebner, A.; Olguin, L. F.; Bratton, D.; Whyte, G.; Huck, W. T. S.; de Mello, A. J.; Edel, J. B.; Abell, C.; Hollfelder, F. *Anal. Chem.* **2008**, *80*, 3890.
(22) Chabert, M.; Dorfman, K. D.; de Cremoux, P.; Roeraade, J.; Viovy, J. L. *Anal. Chem.* **2006**, *78*, 7722.
(23) Gu, S. Q.; Zhang, Y. X.; Zhu, Y.; Du, W. B.; Yao, B.; Fang, Q. *Anal. Chem.* **2011**, *83*, 7570.
(24) Sun, M.; Fang, Q. *Lab Chip* **2010**, *10*, 2864.
(25) Song, H.; Ismagilov, R. F. *J. Am. Chem. Soc.* **2003**, *125*, 14613.
(26) Niu, X. Z.; Gielen, F.; Edel, J. B.; deMello, A. J. *Nat. Chem.* **2011**, *3*, 437.
(27) Miller, O. J.; El Harrak, A.; Mangeat, T.; Baret, J. C.; Frenz, L.; El Debs, B.; Mayot, E.; Samuels, M. L.; Rooney, E. K.; Dieu, P.; Galvan, M.; Link, D. R.; Griffiths, A. D. *Proc. Natl. Acad. Sci. U.S.A.* **2012**, *109*, 378.
(28) Kohler, J. M.; Henkel, T.; Grodrian, A.; Kirner, T.; Roth, M.; Martin, K.; Metze, J. *Chem. Eng. J.* **2004**, *101*, 201.
(29) Abate, A. R.; Hung, T.; Mary, P.; Agresti, J. J.; Weitz, D. A. *Proc. Natl. Acad. Sci. U.S.A.* **2010**, *107*, 19163.
(30) Korczyk, P. M.; Derzsi, L.; Jakiela, S.; Garstecki, P. *Lab Chip* **2013**, *13*, 4096.
(31) Thorsen, T.; Maerkl, S. J.; Quake, S. R. *Science* **2002**, *298*, 580.
(32) Cao, J.; Schneider, S.; Schultheiß, R.; Schober, A.; Köhler, J. M.; Groß, G. A. *Microsyst. Technol.* **2013**, 1.
(33) Schemberg, J.; Grodrian, A.; Romer, R.; Gastrock, G.; Lemke, K. *Eng. Life Sci.* **2009**, *9*, 391.
(34) Cordero, M. L.; Gallaire, F.; Baroud, C. N. *Phys. Fluids* **2011**, 23.
(35) Garstecki, P.; Fuerstman, M. J.; Stone, H. A.; Whitesides, G. M. *Lab Chip* **2006**, *6*, 437.
(36) Seemann, R.; Brinkmann, M.; Pfohl, T.; Herminghaus, S. *Rep. Prog. Phys.* **2012**, *75*, 016601.
(37) Garstecki, P.; Stone, H. A.; Whitesides, G. M. *Phys. Rev. Lett.* **2005**, *94*, 164501 .
(38) Abate, A. R.; Weitz, D. A. *Biomicrofluidics* **2011**, *5*, 014107.
(39) Umbanhowar, P. B.; Prasad, V.; Weitz, D. A. *Langmuir* **2000**, *16*, 347.
(40) Koudelakova, T.; Bidmanova, S.; Dvorak, P.; Pavelka, A.; Chaloupkova, R.; Prokop, Z.; Damborsky, J. *Biotechnol. J.* **2013**, *8*, 32.
(41) Chaloupkova, R.; Prokop, Z.; Sato, Y.; Nagata, Y.; Damborsky, J. *FEBS J.* **2011**, *278*, 2728.
(42) Sato, Y.; Monincova, M.; Chaloupkova, R.; Prokop, Z.; Ohtsubo, Y.; Minamisawa, K.; Tsuda, M.; Damborsky, J.; Nagata, Y. *Appl. Environ. Microbiol.* **2005**, *71*, 4372.
(43) Janssen, D. B. *Curr. Opin Chem. Biol.* **2004**, *8*, 150.
(44) Holloway, P.; Trevors, J. T.; Lee, H. *J. Microbiol. Methods* **1998**, *32*, 31.
(45) Drienovska, I.; Chovancova, E.; Koudelakova, T.; Damborsky, J.; Chaloupkova, R. *Appl. Environ. Microbiol.* **2012**, *78*, 4995.
(46) Koudelakova, T.; Chovancova, E.; Brezovsky, J.; Monincova, M.; Fortova, A.; Jarkovsky, J.; Damborsky, J. *Biochem. J.* **2011**, *435*, 345.
(47) Babtie, A.; Tokuriki, N.; Hollfelder, F. *Curr. Opin. Chem. Biol.* **2010**, *14*, 200.
(48) O'Brien, P. J.; Herschlag, D. *Chem. Biol.* **1999**, *6*, R91.
(49) Bornscheuer, U. T.; Kazlauskas, R. J. *Angew. Chem., Int. Ed.* **2004**, *43*, 6032.
(50) Schindler, J. F.; Naranjo, P. A.; Honaberger, D. A.; Chang, C. H.; Brainard, J. R.; Vanderberg, L. A.; Unkefer, C. J. *Biochemistry* **1999**, *38*, 5772.
(51) Cox, T. T.; Boeker, E. A. *Biochem. J.* **1987**, *245*, 59.
(52) Lim, J.; Gruner, P.; Konrad, M.; Baret, J. C. *Lab Chip* **2013**, *13*, 1472.
(53) Song, H.; Chen, D. L.; Ismagilov, R. F. *Angew. Chem., Int. Ed.* **2006**, *45*, 7336.
(54) Theberge, A. B.; Courtois, F.; Schaerli, Y.; Fischlechner, M.; Abell, C.; Hollfelder, F.; Huck, W. T. S. *Angew. Chem., Int. Ed.* **2010**, *49*, 5846.
(55) Huebner, A.; Srisa-Art, M.; Holt, D.; Abell, C.; Hollfelder, F.; Demello, A. J.; Edel, J. B. *Chem. Commun.* **2007**, 1218.
(56) Srisa-Art, M.; Kang, D. K.; Hong, J.; Park, H.; Leatherbarrow, R. J.; Edel, J. B.; Chang, S. I.; deMello, A. J. *ChemBioChem* **2009**, *10*, 1605.